

# **Fractal form PEDOT/Au assemblies as thin-film neural interface materials**

Katarzyna Krukiewicz<sup>1,2,\*</sup>, Magdalena Chudy<sup>2</sup>, Catalina Vallejo-Giraldo<sup>1</sup>, Małgorzata Skorupa<sup>2</sup>, Daria Więclawska<sup>2</sup>, Roman Turczyn<sup>2</sup>, and Manus Biggs<sup>1</sup>

<sup>1</sup>Centre for Research in Medical Devices (CURAM), Galway Biosciences Research Building, 118 Corrib Village, Newcastle, Galway, Ireland

<sup>2</sup>Department of Physical Chemistry and Technology of Polymers, Silesian University of Technology, M.Strzody 9, 44-100 Gliwice, Poland

\*corresponding author

KatarzynaKrukiewicz

katarzyna.krukiewicz@nuigalway.ie, ORCID ID 0000-0003-0503-0906

## **Abstract**

Electrically conducting polymer formulations have emerged as promising approaches for the development of interfaces and scaffolds in neural engineering, facilitating the development of physicochemically modified constructs capable of cell stimulation through electrical and ionic charge transfer. In particular, topographically functionalized or neuromorphic materials are able to guide the growth of axons and promote enhanced interfacing with neuroelectrodes in vitro. In this study, we present a novel method for the formation of conducting polymer/gold assemblies via a combinational sputter and spin coating technique. The resulting multilayered PEDOT/Au substrates possessed enhanced electrochemical properties as a function of the number of deposited organic/inorganic layers. It was observed that through subsequent electrochemical conditioning it was possible to form neuromorphic fractal-like assemblies of gold particles, which significantly impacted on the electrochemical characteristics of the PEDOT/Au films. PEDOT/Au assemblies were observed to possess unique topographical features, advantageous charge storage capacity ( $34.9 \pm 2.6 \text{ mC/cm}^2$ ) and low electrical impedance ( $30 \pm 2 \Omega$  at 1 kHz). Furthermore, PEDOT/Au assemblies were observed to facilitate the outgrowth of neurites in a mixed ventral mesencephalon cell population and promote an increase in the neurons/astrocytes ratio relative to all experimental groups, indicating PEDOT/Au biomimetic neuromorphic assemblies as promising materials in engineering electrically conductive neural interface systems.

## **Keywords**

conducting polymers; biomimetic materials; neural interfaces; gold particles; PEDOT

## 1. Introduction

Biomimetic materials have received significant interest in biomedical engineering, with a focus on replicating the biochemical and physicochemical properties of the extracellular or the cellular environment [1]. In particular, biomaterials functionalized to present neuromorphic properties have been studied extensively and have been shown to promote neural differentiation, neuron polarity, axon extension and to improve neural tissue regeneration in vitro [2-5]. Encouragingly, recent studies indicate that neuromorphic materials which present micro- and nano- topographical features promote Schwann cell adhesion [6]. Other studies reported on carbon nanotube-based network mimicking the structure of extracellular matrix, for which the majority of neurons selectively grew along CNT patterns and extended further than neurites originally not following the pattern [7].

Conducting polymers, due to their electro-active nature, have emerged as potential materials for neural engineering applications [8]. Critically, multiple conducting polymer chemistries have been previously shown to be biocompatible and have been explored in conjunction with biofunctionalization approaches, whilst serving as conducting mediators for external electrical stimulation with electrical current or electrical fields [9]. In this way, conducting polymers have been explored as organic coatings and scaffolds for the local delivery of bioactive payloads or electrical/ionic signals to promote neural stimulation and regeneration [10-11]. To further enhance material-neural interactions, conducting polymers can be topographically modified with a wide range of advanced techniques, including lithography [12-13] or imprinting [14-15] methods. Gomez et al, [16] recently demonstrated that embryonic hippocampal neurons cultured on neuromorphic micropatterned polypyrrole substrates exhibited enhanced polarization relative to neurons grown on planar materials; polypyrrole features were also found to have the effect on number of cells as well as axon orientation. Conversely, surface chemical and biochemical patterning when applied to conducting polymer surfaces, has also been shown to regulate neuron adhesion, orientation and function in vitro [17]. Critically, synergistic effects have been accomplished by employing dual topographical and chemical functionalization approaches, as described by Jenkins et al who reported on an electrospun nerve guidance conduit functionalized with short peptide (Arg-Gly-Asp) and possessing intraluminal microchannels [18]. The resulting material was shown to guide neurite extension, as well as enhance cell survival and migration.

Recently, conducting polymers have gained attention as neuroelectrode coatings, as a function of their versatility and ease of deposition. Through electrochemical polymerization methods, conducting polymers can be easily grown directly on microscale substrates. This process is, however, limited to conducting substrates, such as platinum, gold or indium-tin oxide, which serve as working electrodes in electrochemical setups. Alternatively, physical techniques, such as spin and spray coating [19] or chemical vapor deposition [20] represent easy, fast and reproducible techniques for the preparation of homogeneous and well-integrated organic and inorganic films on both conducting and non-conducting substrates. Spin-coating in particular has been extensively employed for the

generation of multilayer thin films and porous scaffolds from (3,4-ethylenedioxythiophene):poly(styrene sulfonate) (PEDOT:PSS), an unique water-dispersed conducting polymer with significant application in bioelectronics [21].

Noble metal particles have also been explored extensively for their potential as diagnostics and therapeutic biomaterials [22]. Recent works show that gold nanoparticles in particular can be applied in neural tissue engineering, for the development of neural prosthetic devices and bioelectronic interfaces [23-25]. Through a variety of physical and chemical approaches, noble metal particles have been formulated to create biomimetic architectures with neuromorphic applications [26]. Kim et al [24] recently described the formulation of a microscale radial geometry microelectrode possessing a unique gold nanograin structure, which demonstrated a 10-fold increase in electrical stimulation capability, a 69-fold decrease in impedance, as well as an extremely low noise level and high signal-to-noise ratio. Critically, these neuromorphic and nanoscale features made it possible to evoke action potentials from neurons with the use of small (20–60  $\mu$ A) biphasic current pulses. Similar results have been reported by Seker et al [25], who observed a 25-fold improvement in the electrode–electrolyte impedance and a superior signal-to-noise ratio when conventional gold electrodes were replaced by self-assembled nanoporous gold films. In addition, Zhang et al [23] reported that layer-by-layer assembled films made from gold nanoparticles improved the charge storage capacity relative to non-laminated films by one order of magnitude. Apart from the electrical advantages, gold nanoparticles have been found to enhance neurite outgrowth, modulate neuron depolarization as well as intracellular calcium signaling [27].

Considering the advantages of conducting polymer systems and gold nanoparticle formulations, it was hypothesised that the combination of these two chemistries would result in the formation of composite material possessing properties outperforming both pristine components. In this study, we present a novel multilayer approach for the formation of conducting polymer/gold assemblies through sputter coating of gold and spin coating of the conducting polymer, poly(3,4-ethylenedioxythiophene) (PEDOT). As a result, a multilayered PEDOT/Au structure were formed, possessing properties highly dependent on the number of deposited layers. We show that through electrochemical conditioning it was possible to form neuromorphic fractal-like assemblies of gold particles with variable topography, which impacted significantly on the electrochemical and physicochemical properties of PEDOT/Au films. The biological performance of PEDOT/Au fractal structures were then verified in vitro by ventral mesencephalic (VM) neuron culture studies.

## **2. Materials and Methods**

### *2.1 Fabrication*

A glass support substrate (25 x 25 x 1.0 mm) was used for the fabrication of multi-layered electrodes. Prior to the deposition of multi-layered PEDOT/Au structures, glass slides were sputter-

coated with a thin layer of Pt and pre-treated with an oxygen plasma process (Zepto LF, Diener Electronics) for 10 minutes. The multilayered structure was formed through several consecutive steps comprising spin coating of PEDOT:PSS and sputter coating of Au. PEDOT:PSS aqueous solution was obtained through dissolving 10 mg of PEDOT:PSS pellets (Sigma-Aldrich) in 2 ml of deionized water (Millipore quality). Then, approximately 0.1 ml of the PEDOT:PSS/water solution was placed on the Pt-coated glass and evenly distributed by spin-coating (Laurell Technologies Spin Coater) for 20 s with a speed of 3000 rpm. This resulted in the formation of PEDOT:PSS layer of the thickness of 13 nm. Magnetron sputter-coating was used to subsequently deposit a 10 nm thick layer of gold onto the PEDOT/PSS-covered surfaces. An Emitech K650XT Sputter Coater was used with the operating parameters of 25 mA,  $1 \cdot 10^{-3}$  mbar and 210 s. Seven types of sandwich structures were formed with a consecutively increasing number of layers, starting from PEDOT:PSS and ending with Au. In total, film structures with up to 7 alternating layers of Au and PEDOT were fabricated. Control substrates consisted of Pt-coated glass slides sputter-coated with an Au layer without the presence of PEDOT:PSS.

## *2.2 Conditioning*

To induce the self-arrangement of gold particles and form fractal-like architecture on the surface of PEDOT/Au films, experimental samples were immersed into 0.1 M KCl solution for 10 minutes and subjected to an oscillating potential application performed by means of a PARSTAT 2273 potentiostat and a three-electrode set-up, comprising a multilayer PEDOT/Au structure as a working electrode, Ag/AgCl as a reference electrode and Pt wire as an auxiliary electrode. The applied potential was oscillated between 40 mV and -40 mV for 40 s with a frequency range of 100 kHz to 100 mHz.

## *2.3 Electrochemical characterization*

Electrochemical studies were performed by means of a PARSTAT 2273 potentiostat using cyclic voltammetry and electrochemical impedance spectroscopy (EIS) with the same three-electrode system as described above. EIS spectra were collected in 0.1 M KCl solution within a frequency range from 100 mHz to 100 kHz, with AC amplitude of 40 mV and DC potential equal to 0 V. Cyclic voltammograms (CVs) were collected in 0.1 M KCl solution, within the potential range from -0.8 V to 0.8 V (vs. Ag/AgCl) at 100 mV/s for 5 CV cycles. CVs were used to compare the electrochemical behavior of materials and to determine their charge storage capacity (CSC), calculated as the electric charge integrated under corresponding CV curve during one CV cycle, according to the formula:

$$CSC = \int_{t_1}^{t_2} I(t)dt$$

where  $t_1$  is the beginning of CV cycle,  $t_2$  is the end of CV cycle, and I is the current.

## *2.4 Morphological and chemical characterization*

SEM images were collected by means of Hitachi S-4700 Scanning Electron Microscope operating at 15 kV. Energy Dispersive X-ray Spectroscopy (EDS) was used to confirm the presence and distribution of gold in all PEDOT/Au layered structures. Thickness and roughness of samples were determined by means of a Zygo New view 100 surface profilometer controlled by MicroPlus software. AFM images were collected by means of Dimension 3100 atomic force microscope operated by NanoScope IIIa controller (Digital Instruments, Santa Barbara, CA), in a tapping mode with the use of a TESPA silicon probe (tip height 10 – 15  $\mu\text{m}$ , tip radius < 8 nm, cantilever force constant of 42 N/m). Raman spectra were recorded using a Renishaw InVia confocal microRaman system equipped with laser source operating at 633 nm and a CCD detector (1040 $\times$ 258 resolution), in the spectral range of 250  $\text{cm}^{-1}$  to 1700  $\text{cm}^{-1}$ .

## *2.5 Biological characterization*

### *2.5.1 Ventral Mesencephalic Neuron Culture and Seeding.*

Primary cultures of ventral mesencephalic (VM) neurons were obtained from the mesencephalon of embryonic Sprague–Dawley rats according to a procedure described previously [28]. In short, after dissection from 14-day old rat embryo midbrains, the ventral mesencephalon was mechanically dispersed with a pipette. The cells were cultured in media (Dulbecco's modified Eagle's medium/F12, 33 mM D-glucose, 1 % L-glutamine, 1 % PS, 1 % FCS, supplemented with 2 % B27) and grown in a humidified atmosphere of 5 %  $\text{CO}_2$  at 37  $^\circ\text{C}$  on the surface of PEDOT/Au structures, as well as bare platinum, bare gold and pristine PEDOT:PSS. The specimens were designed to fit 6 well culture plates and sterilized for 2 hours in 70 % ethanol bath. After that, they were washed with Hank's balanced salt solution (HBSS), coated with poly-lysine (PLL) (Sigma) and rinsed three times with distilled (DI) water. After overnight drying, VM cells were seeded onto experimental and control substrates at a density of 50,000 cells per 1  $\text{cm}^2$  and 3 ml of the culture medium was added to each well. Half of the volume was replaced with fresh media every two days for a period of seven days.

### *2.5.2. Immunofluorescent Labeling.*

To visualize neuron and astrocyte cell populations, indirect double-immunofluorescent labeling was used as described previously [29]. In short, after the fixation of cells with 4% paraformaldehyde and 1% of sucrose for 20 min, specimens were washed with PBS and permeabilized with 0.5% Triton X-100 within a buffered isotonic solution (10.3 g sucrose, 0.292 g NaCl, 0.06 g  $\text{MgCl}_2$ , 0.476 g HEPES buffer, 0.5 ml Triton X 100, in 100 ml water, pH 7.2) for 5 min. 1% bovine serum albumin (BSA) in PBS was used to block the non-specific binding sites for 30 min. The specimens were incubated for 2 h with an anti-gial fibrillary acidic protein (GFAP) antibody (Sigma, 1:200, produced in mouse) and anti- $\beta$ -Tubulin III antibody (Sigma, 1:500, produced in rabbit). After triple washing with 0.05% Tween 20/PBS, samples were left for 1 h incubation in the secondary

antibody Alexa Fluor® 488 (Molecular probes, 1:500, goat anti-Mouse IgG / IgA / IgM (H+L)) combined with the secondary antibody Alexa Fluor® 594 (Molecular probes, 1:500, goat anti-Rabbit IgG (H+L)). Samples were washed with PBS, mounted on microscope cover slides and counterstained with slowfade<sup>R</sup> gold antifade reagent with DAPI for nuclear staining.

### *2.5.3. Microscopy and Image Analysis.*

Olympus Fluoview 1000 Confocal Microscope was used to view immunostained samples at a fixed scan size of 1024 by 1024 at a ratio 1:1 and 60x magnification. To analyze the cell density, total number of nuclei corresponding to neurons and astrocytes in an area of 211.97  $\mu\text{m}$  \* 211.97  $\mu\text{m}$  were counted in at least 20 random images taken from each test group and the control group [29]. The quantification of neural lengths was done by analyzing nine random fields of view of three different technical replicas from three different samples using established stereological methods [30], according to the formula:

$$L = nT \frac{\pi}{2}$$

where: L is neurite length ( $\mu\text{m}$ ), n is the number of times neurites intersect with grid lines, T is distance between grid lines ( $\mu\text{m}$ ) [31].

### *2.5.4. Statistical Analysis for Cell Studies.*

The biological experiments were conducted to include at least three biological replicas for each of the test groups and control group. The results were expressed as the mean of the values +/- standard error of the mean, unless otherwise stated. One way ANOVA followed by a Bonferroni test were performed to determine the statistical significance ( $p < 0.05$ ), unless otherwise stated.

### *2.6 Stability evaluation*

The stability of PEDOT/Au multilayer structures and control substrates was determined by comparing the effect of 1000 stimulation cycles on the recorded current density [32]. The conditions of the process were chosen to simulate the parameters used for neural stimulation [33-35]; i.e. a single biphasic potential pulse consisting of a 5-second application of a reduction potential of -0.5 V followed by a 5-second application of an oxidative potential of +0.5 V. To avoid any undesired electrochemical reactions, the voltage was chosen to lie within the water window of the electrodes [32]. To compare the stability of the electrodes, current curves showing five initial (30-35) and five final (995-1000) cycles of electrical stimulation for the each of the experimental and control groups were plotted. Stimulation cycles from 1 to 29 have been omitted because of the necessity of the system to equilibrate. Recorded current curves of the last 5 cycles of stimulation were used to determine the polarization of the bare and modified electrodes.

### 3. Results and Discussion

#### 3.1 Surface characterization

The variability of surface topography of bare metal substrates, pristine PEDOT:PSS and PEDOT/Au multilayer structures is presented in Figure 1. It was observed that sputtered Pt and Au films (Figure 1A and Figure 1B, respectively) formed homogeneous, uniform surfaces with a roughness of only several nm (Table 1). Conversely, when a 13 nm thick layer of PEDOT:PSS was spin-coated onto the Pt seed-layer, the surface became less uniform and more rough, but no notable topography or fractal structures were present, even after the conditioning was performed (Figure 1C). Following a gold sputtering process onto the PEDOT:PSS film (Figure 1D), the conditioning was observed to induce the self-assembly of gold particles aggregated into fractal-like structures, with the chemical composition confirmed by Raman and EDS spectroscopy (Figure 1G,H&I). The Raman spectrum of a representative PEDOT/Au multilayered structure, indicated bands observed at  $1430\text{ cm}^{-1}$ ,  $1368\text{ cm}^{-1}$ ,  $1257\text{ cm}^{-1}$ ,  $1098\text{ cm}^{-1}$ ,  $990\text{ cm}^{-1}$ ,  $702\text{ cm}^{-1}$ ,  $578\text{ cm}^{-1}$  and  $442\text{ cm}^{-1}$  which were attributable to PEDOT and PSS [36]. The bands corresponding to the symmetrical, stretching and inter-ring stretching vibrations of PEDOT were observed at  $1430\text{ cm}^{-1}$ ,  $1368\text{ cm}^{-1}$  and  $1257\text{ cm}^{-1}$ , respectively [37]. The bands at  $990\text{ cm}^{-1}$ ,  $578\text{ cm}^{-1}$  and  $442\text{ cm}^{-1}$  were assigned to oxyethylene ring deformations, and the bands at  $702\text{ cm}^{-1}$  is the symmetric C-S-C deformation [38]. The vibrational modes of PSS are located at  $1098\text{ cm}^{-1}$  and  $990\text{ cm}^{-1}$  [37]. EDS spectrum further confirmed that that the fractal structures were composed of gold.

By increasing the number of layers and the overall gold content in the deposited films (Table 1), the fractal geometries became increasingly developed, with well-defined fractal-like patterns observed in conducting films formed from 6 layers - PEDOT/Au(6L) and 7 layers - PEDOT/Au(7L) (Figure 1E and Figure 1F, respectively). Interestingly, the size of gold particles (Table 1) was also found to vary with the number of layers, from a diameter of 91 nm for a single Au layer, to a diameter of 702 nm for PEDOT/Au(7L). Interestingly, neural interfaces presenting nanoscale roughness profiles, similar to that of the PEDOT/Au films in this study have been shown to promote neuron adhesion in vitro [39]. The Au particles incorporated into PEDOT/Au composites possessing a terminal layer of PEDOT were associated with a reduced diameter, attributed to an investing polymer layer. AFM analysis (Figure 2A) confirmed that the surface of PEDOT/Au(7L) substrates was relatively smooth, with the incorporated Au particles observed to be approx. 50 nm in diameter (Figure 2C). Although the presence of a surface PEDOT:PSS layer made it difficult to observe the Au fractal geometry, AFM phase imaging (Figure 2B) allowed the detection of localized variations in film stiffness and visualization of the spatial distribution of the PEDOT:PSS matrix and Au domains [40]. Since stiff metal regions had a more positive phase shift than a less stiff polymer regions, they appeared brighter in AFM phase imaging [41-42].

Since the process of electrochemical conditioning was necessary to observe the formation of neuromorphic PEDOT/Au structures, it was supposed that the origins of this unique self-assembly

phenomenon arose from the specific interactions between PEDOT:PSS and gold under aqueous conditions. Unlike the majority of conducting polymers, PEDOT:PSS can be easily dispersed in water. When the layered structure of PEDOT:PSS and gold was immersed in aqueous solution, the matrix partially swells and enables gold particles to migrate and agglomerate. This process may be additionally enhanced by matrix polarization with small positive and negative potentials, allowing gold particles embedded into PEDOT:PSS matrix to undergo oxidation and reduction processes, as described by Masitas et al [43]. Furthermore, PEDOT:PSS provided an environment in which gold ions could migrate yet preventing them from moving into bulk solution, facilitating the formation of fractal-like geometries. This was supported by the fact that conducting polymer blends also demonstrate self-assembled fractal-like networks, especially for conducting polymers exhibiting so-called “semi-compatibilization” [44].

Dendritic morphologies have been identified in neural structures at the micro and nanoscale, indicating their functional relevance in neural processes [45] and fractal shapes have been found in retinal [46], thalamic [47] and dorsal horn spinal cord neurons [48]. The presence of topographical fractal-like geometries on conditioned PEDOT/Au multilayer structures may present both electrochemical and biological benefits to neuroelectrode systems. It has been confirmed that fractal interfaces possess improved electrical properties through increasing the electrode surface/interface area, facilitating charge transport and increasing the concentration of charge carriers [49]. The fractal-like arrangement of gold particles, especially in case of PEDOT/Au(6L) (Fig.1E), were observed to resemble dendritic microroots and microbranches. Similar type of topography has been already described by Yang et al, who explored metallic dendrite-like structures in electrically conductive composites as microelectronic devices [50]. Similarly, Dominkovics et al described the fabrication of metallic dendrites through electrochemical migration, and characterized these structures through fractal analysis [45]. Consequently, neural interfaces presenting a nanoscale roughness profile, similar to that observed with the PEDOT/Au films in this study have been shown to promote neuron adhesion *in vitro* [39]. Furthermore, contact guidance of neurites has been observed *in vitro* with neurons cultured on grated topographies as shallow as 14 nm [51]. Interestingly, complex fractal-like topographies have been shown previously to have potential uses for the development of cell culture microsystems, scaffolds for tissue repair and implants for tissue repair in general [52].

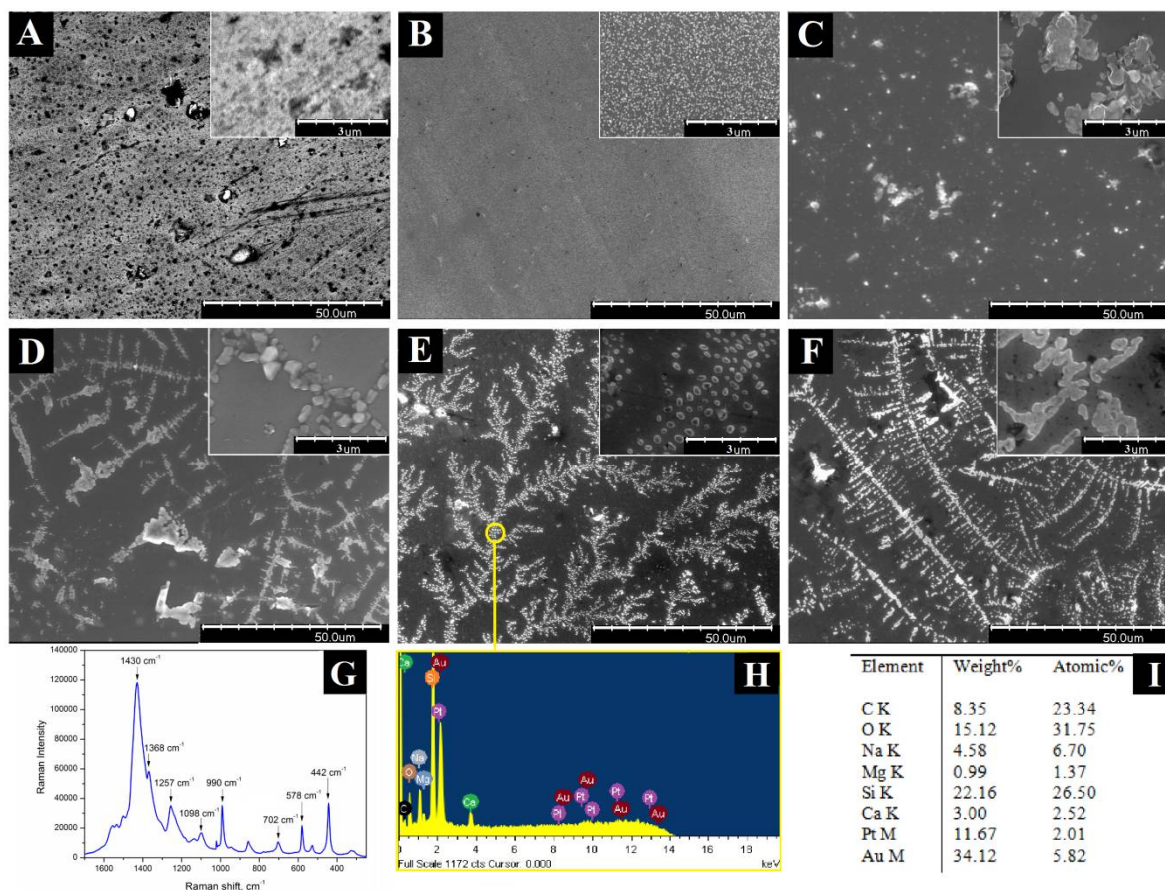


Figure 1. SEM micrographs of magnetron sputtered platinum (A), gold (B), pristine PEDOT:PSS (C), as well as multilayer structures of PEDOT/Au(2L) (D), PEDOT/Au(6L) (E) and PEDOT/Au(7L) (F), (scale bar = 50  $\mu\text{m}$ , high magnification inserts scale bar = 3  $\mu\text{m}$ ). Raman spectrum (G), EDS spectrum (H) and element composition (I) of a fractal structure marked in SEM image of PEDOT/Au(6L).

Sample	Label	Roughness (nm)	Au concentration (atomic %)	Average Au particle diameter(nm)
Pt	Pt	7	-	-
Au	Au	4	95.20	91
P	1L	9	-	-
P: Au	2L	50	7.58	458
P: Au: P	3L	63	5.19	181
P: Au: P: Au	4L	54	25.82	358
P: Au: P: Au: P	5L	53	15.16	271
P: Au: P: Au: P: Au	6L	52	34.12	331
P: Au: P: Au: P: Au: P	7L	47	32.98	702

Table 1. Schematic presentation of multilayer structures of PEDOT/Au, where Pt denotes platinum control substrates, P denotes PEDOT:PSS, Au denotes gold, and the label denotes number of layers, as well as the roughness of the specimens, gold concentration determined using EDS technique and average diameter of Au particles.

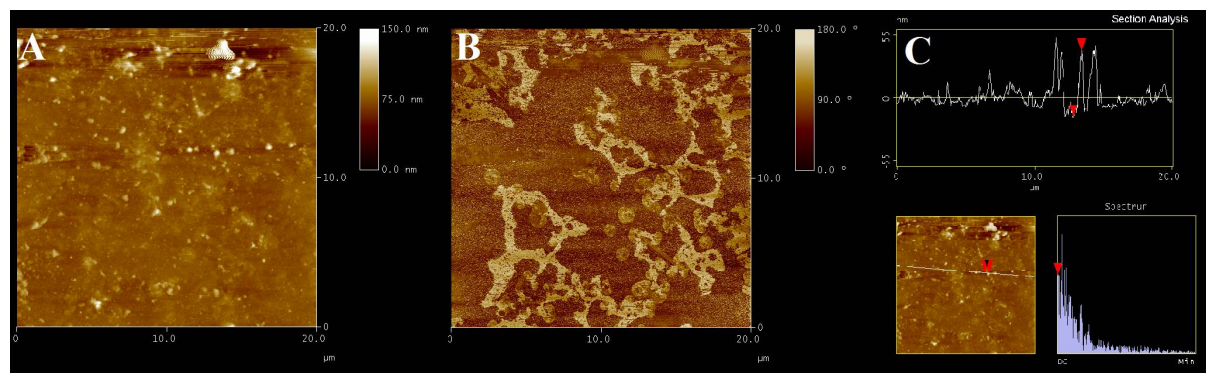


Figure 2. AFM images showing the topography (A), phase (B) and the section height analysis (C) of PEDOT/Au(7L).

### 3.2 Electrochemical performance

A high charge storage capacity (CSC) and low electrochemical impedance profile represent the ideal parameters for the design of neural electrodes [53]. Thus, the selection of the most favourable PEDOT/Au multilayered structure was realized by comparing their CSC and impedance values. The electrochemical performance, with respect to CSC and electrical impedance of layered Au/PEDOT electrodes, was observed to improve with increasing layer number (Figure 3A). The optimum number of layers for electrode fabrication was found to be 7, which demonstrated a high CSC and low electrical impedance, therefore PEDOT/Au(7L) was chosen for further evaluation. Both cyclic voltammograms (Figure 3B) and impedance spectra in form of a Bode plot (Figure 3C) indicated that the electrochemical parameters, i.e. charge storage capacity and impedance, were improved for PEDOT/Au assemblies when compared with bare Pt, bare Au and pristine PEDOT:PSS films. The evolution of the area under CV curve is a visual guide showing the increase in the charge storage capacity. Indeed, a significant increase in CSC from  $1.5 \pm 0.2 \text{ mC/cm}^2$  and  $7.4 \pm 0.5 \text{ mC/cm}^2$  for bare Pt and Au, respectively, through  $15.0 \pm 2.7 \text{ mC/cm}^2$  for PEDOT:PSS, up to  $34.9 \pm 2.6 \text{ mC/cm}^2$  for PEDOT/Au(7L) was observed. Since CSC gives information about the amount of charge that can be stored within the electrode, higher CSC values indicate that a material can produce a higher current density, facilitating a reduced electro-active area and electrode miniaturization [54]. In addition, electrodes presenting a high CSC facilitate neural electrostimulation within a safe voltage range.

Electrochemical impedance values at 1 kHz are used as a benchmark when analyzing the efficacy of conducting polymer electrode systems as the frequency range of 300 Hz to 1 kHz, is relevant in biological stimulation applications [55]. PEDOT/Au assemblies were observed to possess

low electrical impedance profiles over the complete frequency region, significantly lower than all control groups, with an impedance magnitude of  $30 \pm 2 \Omega$  at a frequency of 1 kHz. This observed reduction in electrochemical impedance is of significant concern for the development of electrodes designed for recording of neural electrical activity, providing a high signal-to-noise ratio [25]. Critically, the electrochemical properties of the PEDOT/Au assemblies were observed to improve upon other comparable electroactive materials reported previously. Chen et al. [56] presented PEDOT-coated dry electrodes with a CSC of  $1.28 \text{ mC/cm}^2$  and an electrical impedance of  $2.7 \pm 1.2 \text{ k}\Omega$  at 100 Hz. PEDOT:PSS coatings fabricated by Guex et al [57] induced a decrease in impedance modulus at 1 kHz of more than one order of magnitude (from  $45.27 \pm 2.62 \text{ k}\Omega$  for Pt to  $2.6 \pm 0.66 \text{ k}\Omega$  for PEDOT:PSS of  $0.6 \mu\text{m}$  thickness). Furthermore King et al. [55], reported a CSC of  $26.1 \text{ mC/cm}^2$  and an electrical impedance at 1 kHz of  $319 \Omega$  for PEDOT:PSS. Critically, these coatings exhibited impedance values at least one order of magnitude higher than the 150 nm thick PEDOT/Au assemblies studied herein.

The electroactive materials explored in this study were designed to work at the biological interface, hence it was necessary to assess the polarisation of electrodes as a result of a recurrent physiologically relevant stimulus [32-35]. When subjected to the recurrent biphasic potential pulse of  $+0.5 \text{ V}/-0.5 \text{ V}$  (Fig.3D), all experimental groups displayed an initial ohmic current drop, followed by gradual interfacial polarization. as reported previously [58]. The lowest polarisation, however, was noted for multilayered PEDOT/Au substrates and the presence of neuromorphic PEDOT/Au assemblies were found to reduce electrode polarisation by a factor of three [59].

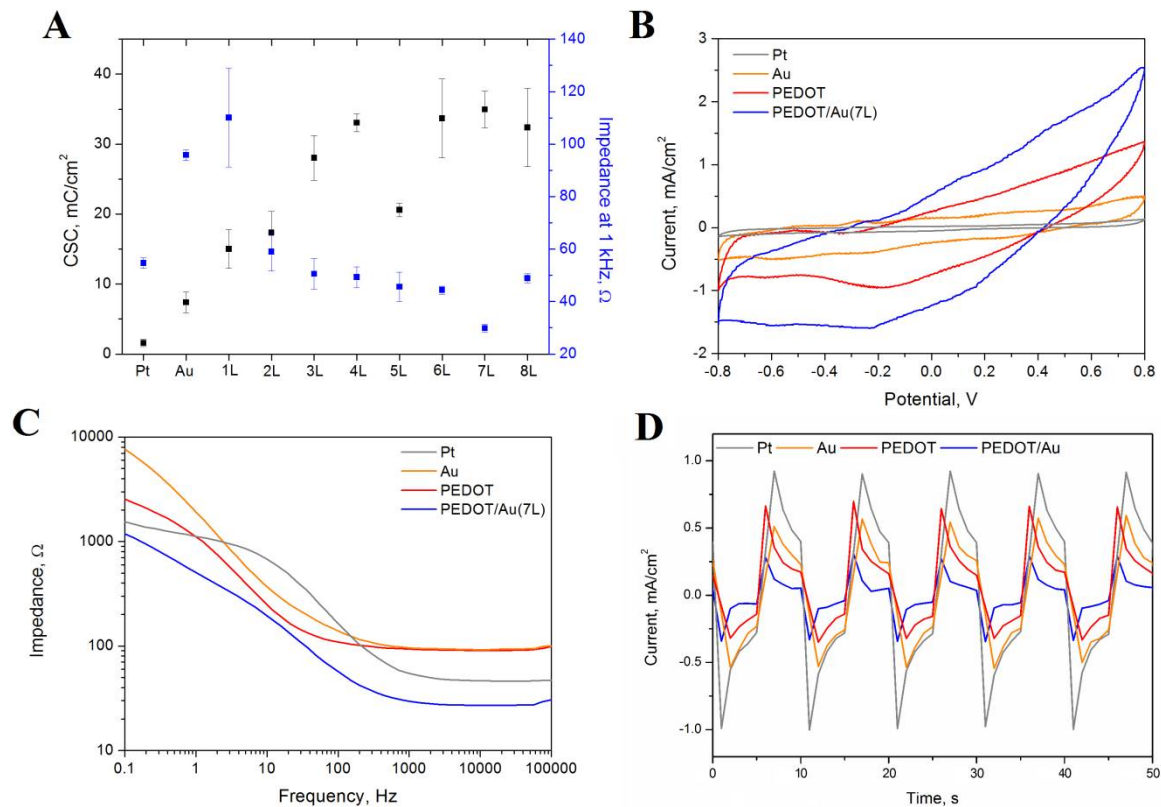


Figure 3. Magnitudes of CSC and electrochemical impedance at 1 kHz frequencies for PEDOT/Au multilayer structures of increasing layer number (A); CV curves (B), Bode plots (C) and polarization current curves (D) for magnetron sputtered Pt, magnetron sputtered Au, pristine PEDOT:PSS and a representative PEDOT/Au(7L) multilayered structures, indicating the low impedance and high charge storage capacity of PEDOT/Au fractal assemblies.

### 3.3 Cytocompatibility studies

Figure 4A-D shows representative micrographs of neuron and astrocyte cells identified in a primary mixed cell population derived from embryonic VM explants. Cells were cultured over a period of seven days on magnetron sputtered Pt, magnetron sputtered Au, pristine PEDOT:PSS and PEDOT/Au assemblies. Numerical and morphometric analysis of neural and astrocyte populations obtained from epi fluorescent microscopy images revealed significant differences in the astrocyte-to-neuron ratio as well as average neurite length in cells cultured on PEDOT/Au with respect to all control groups, alluding to the role of fractal-like geometry in modulating cell function [60]. A significant increase in the astrocyte-to-neuron ratio was observed in VM cells following 7 days in culture on PEDOT/Au assemblies, relative to magnetron sputtered Pt and Au films, indicating the positive effect of the inherent PEDOT nanoroughness, and of the self-affine neuromorphic arrangement obtained with PEDOT/Au assemblies on the persistence of neurons (Figure 4E). Both PEDOT and PEDOT/Au substrates were found to support the highest percentage of neurons (74.5 %

and 80.4%, respectively) and the lowest percentage of astrocytes (25.5 % and 19.6 %, respectively), with no statistical difference between these two substrates and comparable with other structured neural interface materials [29,61-63].

The neurite outgrowth length was also quantified in  $\beta$ -tubulin III positive cells cultured on all experimental and control groups (Figure 4F), and was observed to increase from  $123 \pm 6 \mu\text{m}$  on Pt;  $156 \pm 6 \mu\text{m}$  on Au; through  $244 \pm 4 \mu\text{m}$  on pristine PEDOT films, to  $303 \pm 12 \mu\text{m}$  on PEDOT/Au assemblies. These results agree with previous data which shows a similar increase in neurite outgrowth on gold with respect to the platinum [64], as well as facilitated neurite growth on materials containing PEDOT [65-66]. A synergetic effect is observed in this study with dual PEDOT/Au assemblies. The enhanced neurite outgrowth is hypothesized to arise from the advantageous chemistries of PEDOT and Au, in conjunction with the physical cues arising from the biomimetic topography of conditioned PEDOT/Au substrates. This effect was reported previously by Kofron et al. [1] and Dubey et al. [51], employing substrates with anisotropic topographies although the role of randomly, self-affine fractal-like PEDOT/Au substrates on stimulating the neural cell machinery to support outgrowth and adhesion has not been previously described.

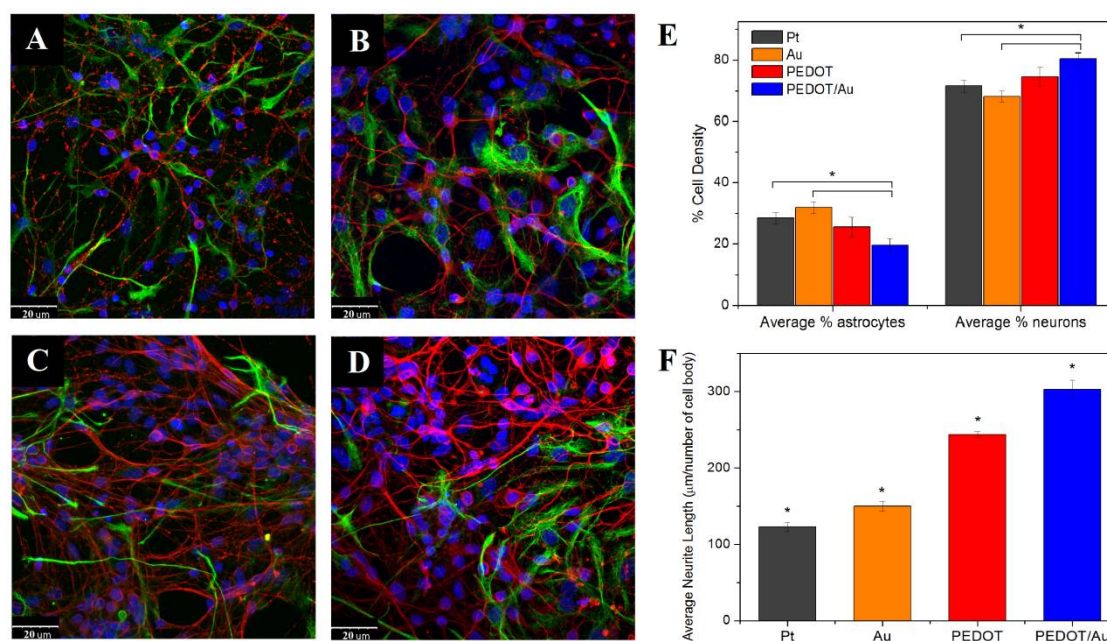


Figure 4. Fluorescent images of primary ventral mesencephalic (VM) mixed cell population cultured for seven days on each of the experimental and control groups: magnetron sputtered Pt (A), magnetron sputtered Au (B) pristine PEDOT:PSS (C) and PEDOT/Au assemblies (D); neurons are visualized by anti  $\beta$ -tubulin III (red), astrocyte cells by anti-GFAP (green) and nuclei by DAPI(blue); the scale bar represents 20  $\mu\text{m}$ . Cell density (%) analysis of astrocyte and neuron presence on each of the experimental and control group (E) and neural length analysis of the experimental and control group (F);  $\star = p < 0.05$ ,  $N=3$ .

### *3.4 Stability evaluation*

To verify the electrochemical stability of PEDOT/Au fractal assemblies, accelerated electrical stimulation with 1000 physiologically relevant stimulation cycles were performed with biphasic potential pulses of 0.5 V and -0.5 V applied alternatively for a period of 5 s each. Figure 5A-D compares current flow through experimental assemblies and control films in five initial (after the first, non-equilibrium phase) and five final cycles of 1000 cycles of electrical stimulation. The highest stability was observed for magnetron sputtered Pt electrodes, however, the maximum currents achieved in each stimulation cycle are of similar magnitudes irrespectively of the stage of the process. The least stable electrochemical behavior was observed in magnetron sputtered Au electrodes, in which the fluctuations in currents could be observed within the initial stimulation cycles. Both PEDOT and PEDOT/Au demonstrated moderate electrochemical stability, between that of magnetron sputtered Pt and Au. Nevertheless, the comparison of CV curves obtained before and after stability evaluation for PEDOT (Figure 5G) and PEDOT/Au assemblies (Figure 5H) indicate the consistency in their electrochemical behavior and charge storage capacity, confirming the favourable electrochemical stability of these materials for neural tissue applications.

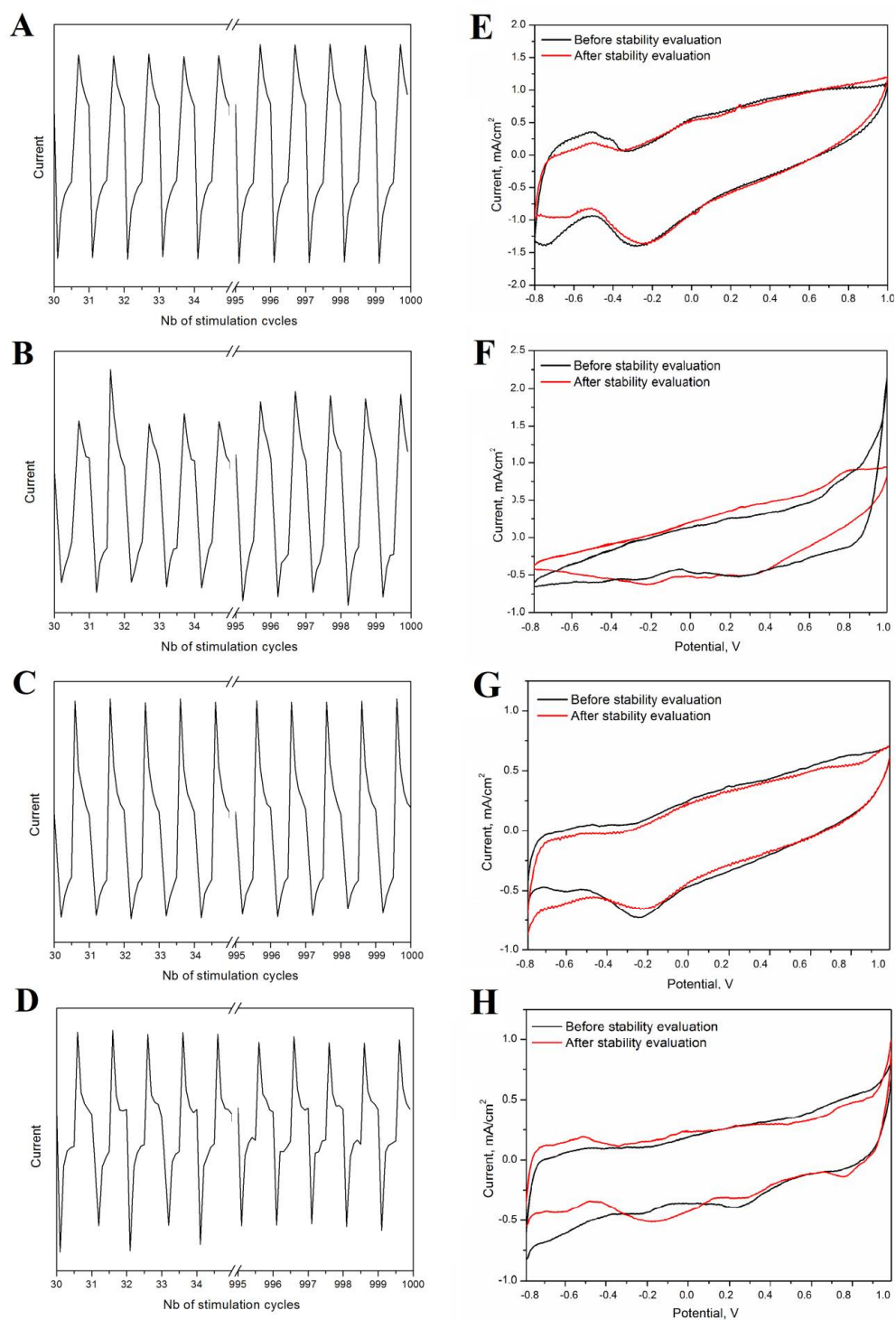


Figure 5. Current plots showing initial (30-35) and final (995-1000) cycles of electrical stimulation for each of the experimental and control groups, i.e. magnetron sputtered Pt (A), magnetron sputtered Au (B) pristine PEDOT:PSS (C) and PEDOT/Au (D). The comparison of CV curves collected before and after performing 1000 stimulation cycles for magnetron sputtered Pt (E), magnetron sputtered Au (F), pristine PEDOT:PSS (G) and PEDOT/Au(H) indicate the electrochemical stability of these electrodes.

## 4 Conclusions

In this study, it was shown that organic-inorganic composites formulated of alternating PEDOT and sputtered gold films form fractal-like Au particle assemblies following conditioning under aqueous conditions. Self-assembled neuromorphic substrates demonstrated superior electrochemical and biological properties relative to pristine Pt, Au and PEDOT electrodes. PEDOT/Au assemblies were observed to possess advantageous electrical properties, in terms of high charge storage capacity and low electrical impedance. Owing to the unique microtopography of PEDOT/Au assemblies, these films induced a significant increase in neurite outgrowth in VM derived neural populations, and maintained the highest neuron-to-astrocyte surface coverage ratio among all experimental and control groups. Furthermore, PEDOT/Au films were fabricated via a facile sputter coating and spin coating approach, a technique which can be scaled-up for industrial applications and demonstrates promise for the fabrication of applied neural interfaces.

## Acknowledgements

This publication has emanated from research conducted with the financial support of Science Foundation Ireland (SFI) and is co-funded under the European Regional Development Fund under Grant Number 13/RC/2073. This project has received funding from the European Union's Horizon 2020 research and innovation programme under the Marie Skłodowska-Curie grant agreement No 713690 and SFI Technology Innovation Development Programme, grant no. 15/TIDA/2992. The authors acknowledge the facilities and scientific and technical assistance of the Centre for Microscopy & Imaging at the National University of Ireland Galway, a facility that is funded by NUIG and the Irish Government's Programme for Research in Third Level Institutions, Cycles 4 and 5, National Development Plan 2007-2013.

## Literature

1. Kofron CM, Liu YT, Lopez-Fagundo CY, Mitchel JA and Hoffman-Kim D 2010 Neurite Outgrowth at the Biomimetic Interface *Ann. Biomed. Eng.* 38(6) 2210-25
2. Zhu W, O'Brien C, O'Brien JR and Zhang LG 2014 3D nano/microfabrication techniques and nanobiomaterials for neural tissue regeneration *Nanomedicine (Lond)* 9(6) 859-75
3. Alvarez Z, Castano O, Castells AA, Mateos-Timoneda MA, Planell JA, Engel E and Alcantara S 2014 Neurogenesis and vascularization of the damaged brain using a lactate-releasing biomimetic scaffold *Biomaterials* 35(17) 4769-81
4. Tran RT, Choy WM, Cao H, Qattan I, Chiao JC, Ip WY, Yeung KW and Yang J 2014 Fabrication and characterization of biomimetic multichanneled crosslinked-urethane-doped polyester tissue engineered nerve guides *J. Biomed. Mater. Res. A* 102(8) 2793-804

5. Zhu B, Luo SC, Zhao H, Lin HA, Sekine J, Nakao A, Chen C, Yamashita Y and Yu HH 2014 Large enhancement in neurite outgrowth on a cell membrane mimicking conducting polymer *Nature Commun.* 5 4523
6. Bruder JM, Lee AP and Hoffman-Kim D 2007 Biomimetic materials replicating Schwann cell topography enhance neuronal adhesion and neurite alignment in vitro *J. Biomater. Sci. Polym. Ed.* 18(8) 967-82
7. Jang MJ, Namgung S, Hong S and Nam Y 2010 Directional neurite growth using carbon nanotube patterned substrates as a biomimetic cue *Nanotechnology* 21, 235120
8. Vallejo-Giraldo C, Kelly A and Biggs MJ 2014 Biofunctionalisation of electrically conducting polymers *Drug Discov. Today* 19(1) 88-94
9. Lee JY 2013 Electrically Conducting Polymer Based Nanofibrous Scaffolds for Tissue Engineering Applications *Polym Rev.* 53 443-59
10. Sudwilai T, Ng JJ, Boonkrai C, Israsena N, Chuangchote S and Supaphol P 2014 Polypyrrole-coated electrospun poly(lactic acid) fibrous scaffold: effects of coating on electrical conductivity and neural cell growth *J. Biomater. Sci.* 25(12) 1240-52
11. Lee JY, Bashur CA, Milroy CA, Forciniti L, Goldstein AS and Schmidt CE 2012 Nerve Growth Factor-Immobilized Electrically Conducting Fibrous Scaffolds for Potential Use in Neural Engineering Applications *IEEE Trans. Nanobioscience* 11(1) 15-21
12. Tiu BD, Pernites RB, Foster EL and Advincula RC 2015 Conducting polymer-gold co-patterned surfaces via nanosphere lithography *J. Colloid Interface Sci.* 459 86-96
13. Chakraborty A, Parthasarathi G and Luo C 2007 Investigation of the conducting polymer microsensors generated using an intermediate-layer lithography method *Proc. SPIE – International Society for Optical Engineering* 6556 65560Y
14. Meier R, Markl F, Birkenstock C and Muller-Buschbaum P 2012 Film thickness controllable wet-imprinting of nanoscale channels made of conducting or thermoresponsive polymers *J. Mater. Chem.* 22 192-8
15. Vallejo-Giraldo C, Dowd E, Papy-Garcia D, Pandit A and Biggs MJ 2016 Functionalized PEDOT polymeric coatings for neuroelectrodes: topographical and biological strategies *Front. Bioeng. Biotechnol. Conference Abstract: 10th World Biomaterials Congress*
16. Gomez N, Lee JY, Nickels JD and Schmidt CE 2007 Micropatterned Polypyrrole: A Combination of Electrical and Topographical Characteristics for the Stimulation of Cells *Adv. Funct. Mater.* 17(10) 1645-53
17. Ho D et al. 2015 Hierarchical Patterning of Multifunctional Conducting Polymer Nanoparticles as a Bionic Platform for Topographic Contact Guidance *ACS Nano* 9(2) 1767-74
18. Jenkins PM, Laughter MR, Lee DJ, Lee YM, Freed CR and Park D 2015 A nerve guidance conduit with topographical and biochemical cues: potential application using human neural stem cells *Nanoscale Res. Lett.* 10(1) 972

19. Zabihi F, Xie Y, Gao S and Eslamian M 2015 Morphology, conductivity, and wetting characteristics of PEDOT:PSS thin films deposited by spin and spray coating *Appl. Surf. Sci.* 338 163-77
20. Asatekin A, Barr MC, Baxamusa SH, Lau KKS, Tenhaeff W, Xu J and Gleason KK 2010 Designing polymer surfaces via vapor deposition *Materials Today* 13(5) 26-33
21. El Mahmoudy M, Inal S, Charrier A, Uguz I, Malliaras GG and Sanaur S 2017 Tailoring the Electrochemical and Mechanical Properties of PEDOT:PSS Films for Bioelectronics. *Macromol. Mater. Eng.* 302 (5) 1600497
22. Rai M, Ingle AP, Birla S, Yadav A and Santos CA 2016 Strategic role of selected noble metal nanoparticles in medicine *Crit. Rev. Microbiol.* 42(5) 696-719
23. Zhang H, Shih J, Zhu J and Kotov NA 2012 Layered Nanocomposites from Gold Nanoparticles for Neural Prosthetic Devices *Nano Lett.* 12(7) 3391-98
24. Kim R, Hong N and Nam Y 2013 Gold nanograin microelectrodes for neuroelectronic interfaces *Biotechnol J* 8(2) 106-14
25. Seker E, Berdichevsky Y, Begley MR, Reed ML, Staley KJ and Yarmush ML 2010 The fabrication of low-impedance nanoporous gold multiple-electrode arrays for neural electrophysiology studies *Nanotechnology* 21(12) 125504
26. Bose SK, Mallinson JB, Gazoni RM and Brown SA 2017 Stable Self-Assembled Atomic-Switch Networks for Neuromorphic Applications *IEEE Transactions on Electronic Devices* 64(12) 5194-201
27. Paviolo C and Stoddart PR 2017 Gold Nanoparticles for Modulating Neuronal Behavior *Nanomaterials (Basel)* 24(7) E92
28. Vallejo-Giraldo C et al. 2017 Preparation of Cytocompatible ITO Neuroelectrodes with Enhanced Electrochemical Characteristics Using a Facile Anodic Oxidation Process *Adv. Funct. Mater.* 1605035
29. Vallejo-Giraldo C et al. 2016 Polyhydroxyalkanoate/carbon nanotube nanocomposites: flexible electrically conducting elastomers for neural applications *Nanomedicine (Lond)* 11(19) 2547-63
30. O'Keefe GW, Dockery P and Sullivan AM 2004 Effects of growth/differentiation factor 5 on the survival and morphology of embryonic rat midbrain dopaminergic neurones in vitro. *J. Neurocytology* 33(5) 479-88
31. Kavanagh ET, Loughlin JP, Herbert KR, Dockery P, Samali A, Doyle KM and Gorman AM 2006 Functionality of NGF-protected PC12 cells following exposure to 6-hydroxydopamine. *Biochem. Biophys. Res. Comm.* 351(4) 890-5
32. Negi S, Bhandari R, Rieth L, Van Wegenen R and Solzbacher F 2010 Neural Electrode Degradation from Continuous Electrical Stimulation: Comparison of Sputtered and Activated Iridium Oxide *J. Neurosci. Methods* 186(1) 8-17

33. Merrill DR, Bikson M and Jefferys JG 2005 Electrical stimulation of excitable tissue: design of efficacious and safe protocols. *J. Neurosci. Methods* 141(2) 171-98
34. Pieber K, Herceg M, Paternostro-Sluga T and Schuhfried O 2015 Long Pulse Biphasic Electrical Stimulation of Denervated Muscle. *J. Neuroeng. Rehabil.* 12 51
35. Goo Y and Ye J 2008 Comparison of Electrical Stimulation Parameters for Normal and Degenerate Mouse Retina. *IOVS* 49(13) 3040
36. Sakamoto S, Okumura M, Zhao Z and Furukawa Y 2005 Raman spectral changes of PEDOT–PSS in polymer light-emitting diodes upon operation. *Chem. Phys. Lett.* 412 (4-6) 395-398
37. Chang SH, Chiang CH, Kao FS, Tien CL and Wu CG 2014 Unraveling the Enhanced Electrical Conductivity of PEDOT:PSS Thin Films for ITO-Free Organic Photovoltaics. *IEEE Photonics J.* 6 (4) 8400307
38. Garreau S, Louarn G, Buisson JP, Froyer G and Lefrant S 1999 In Situ Spectroelectrochemical Raman Studies of Poly(3,4-ethylenedioxythiophene) (PEDT). *Macromolecules* 32(20) 6807-12
39. Khan SP, Auner GG and Newaz GM 2005 Influence of nanoscale surface roughness on neural cell attachment on silicon. *Nanomedicine: NBM* 1(2) 125-9
40. Nagao E and Dvorak JA 1999 Phase Imaging by Atomic Force Microscopy: Analysis of Living Homoiothermic Vertebrate Cells. *Biophys J* 76(6) 3289-97
41. Magonov SN, Elings V and Whangbo MH 1997 Phase imaging and stiffness in tapping-mode atomic force microscopy. *Sur Sci Lett* 375 L385–L391
42. Whangbo MH, Magonov SN and Bengel H 1997 Tip-sample force interactions and surface stiffness in scanning probe microscopy. *Probe Microsc.* 1 23-42.
43. Masitas RA and Zamborini FP 2012 Oxidation of Highly Unstable <4 nm Diameter Gold Nanoparticles 850 mV Negative of the Bulk Oxidation Potential. *J. Am. Chem. Soc.* 134(11) 5014-7
44. Hopkins AR and Reynolds JR 2000 Crystallization Driven Formation of Conducting Polymer Networks in Polymer Blends. *Macromolecules* 33(14) 5221-26
45. Werner G 2010 Fractals in the Nervous System: Conceptual Implications for Theoretical Neuroscience. *Front. Physiol.* 1(15) 15
46. Caserta F, Stanley HE, Eldred WD, Daccord G, Hausman RE and Nittmann 1990 Physical mechanisms underlying neurite outgrowth: A quantitative analysis of neuronal shape. *J Phys Rev Lett.* 64(1) 95-8.
47. Kniffki KD, Pawlak M and Vahle-Hinz C 1994 Fractal Dimensions and Dendritic Branching of Neurons in the Somatosensory Thalamus. In: Nonnenmacher T.F., Losa G.A., Weibel E.R. (eds) *Fractals in Biology and Medicine. Mathematics and Biosciences in Interaction.* Birkhäuser, Basel

48. Milosevic NT, Ristanovic D, Stankovic JB, Gudovic R 2007 Fractal analysis of dendritic arborisation patterns of stalked and islet neurons in substantia gelatinosa of different species *Fractals* 15(1) 1-7
49. Chamousis RL et al. 2014 Effect of fractal silver electrodes on charge collection and light distribution in semiconductingorganic polymer films.*J. Mater. Chem. A* 2 16608-16
50. Yang C, Cui X, Zhang Z, Chiang SW, Lin W, Duan H, Li J, Kang F and Wong CP 2015 Fractal dendrite-based electrically conductive composites for laser-scribed flexible circuits *Nat Commun.* 6, 8150.
51. Dubey N, Letourneau PC and Tranquillo RT 1999 Guided Neurite Elongation and Schwann Cell Invasion into Magnetically Aligned Collagen in Simulated Peripheral Nerve Regeneration*Exp. Neurol.* 158(2) 338-50
52. Diaz LA, Pareja-Sanchez B, Murillo G and Sotillo J 2013 Fractals in tissue engineering: toward biomimetic cell-culture matrices, microsystems and microstructured implants*Expert Rev. Med. Devices* 10(5) 629-48
53. Aregueta-Robles UA, Woolley AJ, Poole-Warren LA, Lovell NH and Green RA 2014 Organic electrode coatings for next-generation neural interfaces *Front Neuroeng.* 7(15) 1-18
54. Gong CA, Syu WJ, Lei KF and Hwang YS 2016 Development of a Flexible Non-Metal Electrode for Cell Stimulation and Recording*Sensors (Basel)* 16(10) E1613
55. King ZA, Shaw CM, Spanninga SA and Martin DC 2011 Structural, chemical and electrochemical characterization of poly(3,4-ethylenedioxythiophene) (PEDOT) prepared with various counter-ions and heat treatments *Polymer* 52 1302-8
56. Chen Y, Pei W, Chen S, Wu X, Zhao S, Wang H and Chen H 2013 Poly(3,4-ethylenedioxythiophene) (PEDOT) as interface material for improving electrochemical performance of microneedles array-based dry electrode*Sensors Actuat. B: Chem.* 188 747-56
57. Guex AA, Vachicouras N, Hight AE, Brown MC, Lee DJ and Lacour SP 2015 conducting polymer electrodes for auditory brainstem implants *J Mater Chem B, Mater Bio Med* 3, 5021-7
58. Wilks SJ, Richardson-Burns SM, Hendricks JL, Martin DC and Otto KJ 2009 Poly(3,4-ethylenedioxythiophene) as a micro-neural interface material for electrostimulation *Front Neuroengineering* 2, 7
59. Pranti AS, Schander A, Bodecker A and Lang W 2017 Highly Stable PEDOT:PSS Coating on Gold Microelectrodes with Improved Charge Injection Capacity for Chronic Neural Stimulation *Proceedings* 1(4) 492
60. Gentile F, Medda R, Cheng L, Battista E, Scopelliti PE, Milani P, Cavalcanti-Adam EA and Decuzzi P 2013 Selective modulation of cell response on engineered fractal silicon substrates *Sci. Rep.* 3 1461

61. Cui X, Hetke JF, Wiler JA, Anderson DJ and Martin DC 2001 Electrochemical deposition and characterization of conducting polymer polypyrrole/PSS on multichannel neural probes *Sens. Actuators A* 93 8-18
62. Webster TJ, Waid MC, McKenzie JL, Price RL and Ejiogor JU 2003 Nano-biotechnology: carbon nanofibres as improved neural and orthopaedic implants *Nanotechnol.* 15 48
63. Chapman CAR, Wang L, Chen H, Garrison J, Lein PJ and Seker E 2017 Nanoporous Gold Biointerfaces: Modifying Nanostructure to Control Neural Cell Coverage and Enhance Electrophysiological Recording Performance *Adv. Funct. Mater.* 27(3) 1604631
64. Brors D, Aletsee C, Schwager K, Mlynski R, Hansen S, Schafers M, Ryan AF and Dazert S 2002 Interaction of spiral ganglion neuron processes with alloplastic materials in vitro *Hear Res.* 167(1-2) 110-21
65. Wang S, Guan S, Wang J, Liu H, Liu T, Ma X and Cui Z 2016 Fabrication and characterization of conductive poly (3,4-ethylenedioxythiophene) doped with hyaluronic acid/poly (L-lactic acid) composite film for biomedical application *J. Biosci. Bioeng.* 123(1) 116-25
66. Kim S, Oh WK, Jeong YS and Jang J 2012 Dual-Functional Poly(3,4-ethylenedioxythiophene)/MnO<sub>2</sub> Nanoellipsoids for Enhancement of Neurite Outgrowth and Exocytosed Biomolecule Sensing in PC12 Cells *Adv. Funct. Mater.* 23(15) 1947-56